

Chapter 5

Characteristics of Graphene/Reduced Graphene Oxide



Pankaj Chamoli, Soma Banerjee, K. K. Raina and Kamal K. Kar

Abstract Graphene, the thinnest two-dimensional material, is extensively explored by interdisciplinary fields of research communities due to the excellent electronic, mechanical, optical and thermal properties. This chapter provides a comprehensive review of the structure, synthesis, properties and applications of graphene/reduced graphene oxide. Graphene, the one atomic thick layer of sp^2 hybridized carbon atoms arranged in honeycomb lattice, is the building block of all carbon materials such as graphite, carbon nanotubes and fullerenes. It can be synthesized by different techniques such as micromechanical cleavage, exfoliation and chemical vapour deposition. It has also been commonly synthesized from the reduction in graphene oxide. The reduction of graphene oxide again is also carried out either by using hazardous chemicals or by green approach. This chapter also discusses the properties of graphene/reduced graphene oxide, which makes them a potential material in diverse applications. The potential fields of applications of graphene/reduced graphene oxide include medicine, electronics, energy devices, sensors, environmental and many more.

P. Chamoli · K. K. Raina

Department of Physics, DIT University, Dehradun, Uttarakhand, India
e-mail: pchamoli83@gmail.com

K. K. Raina

e-mail: kkraina@gmail.com

P. Chamoli · S. Banerjee · K. K. Kar (✉)

Advanced Nanoengineering Materials Laboratory, Materials Programme, Indian Institute of Technology Kanpur, Kanpur 208016, India
e-mail: kamalkk@iitk.ac.in

S. Banerjee

e-mail: somabanerjee27@gmail.com

K. K. Kar

Advanced Nanoengineering Materials Laboratory, Material Science Programme and Department of Mechanical Engineering, Indian Institute of Technology Kanpur, Kanpur 208016, India

© Springer Nature Switzerland AG 2020

K. K. Kar (ed.), *Handbook of Nanocomposite Supercapacitor Materials I*,
Springer Series in Materials Science 300,
https://doi.org/10.1007/978-3-030-43009-2_5

5.1 Introduction

Carbon is the foundation of organic chemistry and the key material for life. Due to flexibility of bond formation, carbon-based systems are composed of a number of structures of wide physical properties. Graphene/reduced graphene oxide, the exciting material of modern age, has found interest by the scientific community of interdisciplinary fields due to the remarkable physical properties and chemical tunability opening the provisions of vast applications in the field of physics, chemistry and materials science. It plays a decisive role to determine the electronic properties of carbon allotrope and can be considered as a honeycomb structure made of hexagons. Graphene, the mother of all carbon allotrope, has been unknowingly produced by someone, who writes with a pencil. However, it has been recognized much later. The main reason behind the fact is that the existence of graphene in the free state is questionable and no experimental tool has been available to detect one-atom-thick graphene layer from the pencil debris.

A group of researchers at Manchester University, Andre Geim and Konstantin Novoselov, have successfully isolated a single layer of graphene by mechanically cleaving graphite crystal [1]. Graphene is the 'thinnest' 2D material and exhibits extraordinary electrical, optical, mechanical and thermal properties [1, 2]. It has inspired the development of many envisaged modern devices due to the excellent electrical conductivity, transparency along with flexibility such as roll-up and flexible electronics, energy storage materials, energy conversion materials, polymer composites and transparent conducting film/electrodes [3, 4]. Graphene, the wonder material, exhibits a theoretical specific surface area of $2630 \text{ m}^2 \text{ g}^{-1}$ with excellent intrinsic mobility of $200,000 \text{ cm}^2 \text{ v}^{-1} \text{ s}^{-1}$. It exhibits high Young's modulus and thermal conductivity values of $<1 \text{ TPa}$ and $<5000 \text{ W m}^{-1} \text{ K}^{-1}$, respectively, with good optical transmittance ($<97.7\%$) [5–7]. The excellent electronic properties of graphene make them a suitable material as transparent conductive electrodes [8].

5.2 Structure of Graphene

Graphene is the structural building block of all graphitic forms, including 3D graphite, 2D graphene, 1D carbon nanotubes and 0D fullerenes. It is one atomic thick layer of sp^2 hybridized carbon atoms arranged in a honeycomb lattice with C–C bond lengths of 1.42 \AA and partially filled pi-orbitals above and below the plane of sheet [9]. Graphite is the form of numerous graphene sheets stacked together with an interplanar spacing of 3.35 \AA . You will be happy to know that approximately three million layers of stacked graphene sheets are present in a 1-mm-thick graphite crystal [2]. The categorization of graphene has been made on the basis of electronic properties and generally prefixed by 'monolayer', 'bilayer' or 'few-layer' (generally excepted to be <10 layers) graphene.

Monolayer graphene generally exists without stacking of sheets, and 4–6 few-layer graphene can have a number of stacking arrangements, including ABAB (named as Bernal stacking), ABCABC (called rhombohedral stacking) and sometimes AAA stacking. In general, graphene is a planar structure of carbon atom arranged in a hexagonal lattice and has been seen as a triangular lattice with a basis of two atoms per unit cell (Fig. 5.1). The lattice vectors can be written as [10]:

$$a_1 = \frac{a}{2}(3, \sqrt{3}) \quad a_2 = \frac{a}{2}(3, -\sqrt{3}) \quad (5.1)$$

where $a \sim 1.42 \text{ \AA}$ is the C–C bond distance.

The reciprocal-lattice vectors are represented by

$$b_1 = \frac{2\pi}{3a}(1, \sqrt{3}) \quad b_2 = \frac{2\pi}{3a}(1, -\sqrt{3}) \quad (5.2)$$

The two points K and K' are at the corners of the graphene Brillouin zone, named as Dirac points and positions in momentum space are represented by

$$K = \left(\frac{2\pi}{3a}, \frac{2\pi}{3\sqrt{3}a} \right) \quad K' = \left(\frac{2\pi}{3a}, -\frac{2\pi}{3\sqrt{3}a} \right) \quad (5.3)$$

The three nearest-neighbour vectors in real space are written as

$$\delta_1 = \frac{a}{2}(1, \sqrt{3}) \quad \delta_2 = \frac{a}{2}(1, -\sqrt{3}) \quad \delta_3 = a(1, 0) \quad (5.4)$$

with the six second nearest neighbours are located at

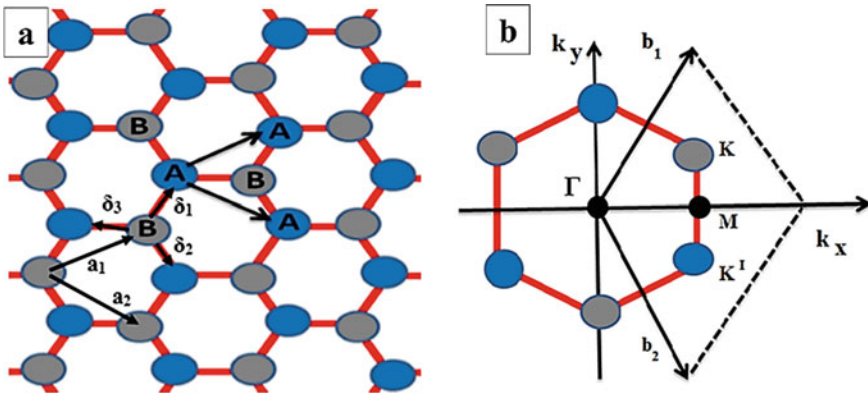


Fig. 5.1 **a** Triangular sublattice of graphene A having three nearest neighbours in sublattice and B vice versa, **b** K and K' as the Dirac points. Redrawn and reprinted with permission from [10]

$$\delta'_1 = \pm a_1 \quad \delta'_2 = \pm a_2 \quad \delta'_3 = \pm(a_2 - a_1) \quad (5.5)$$

5.3 Synthesis of Graphene/Reduced Graphene Oxide

Since graphene was isolated using the scotch tape method [1], many processes have been explored/demonstrated to produce few-to-single-layer graphene. The main concern is to synthesize high carrier mobility and low defect density in graphene. Hence, different synthesis approaches of continuous growth of few-layer graphene have been explored such as exfoliation, chemical vapour deposition and wet chemical approach. Few of them have been discussed here. Moreover, chemical vapour deposition gives a great impact over thermal exfoliation due to the defect-free synthesis of graphene. Wet chemical approach is another widely method of graphene production due to the provisions of large-scale synthesis at a low cost.

5.3.1 Exfoliation Approach

5.3.1.1 Micromechanical Cleavage

A scotch tape method developed by Geim and Novoselov is known as ‘micromechanical cleavage’, involves adhesive tape assisted peeling off a piece of graphite [11]. In this method, the monolayer graphene has been produced with high structural quality. In fact, this approach provides the best graphene structure in terms of high purity, low defects and optoelectronic properties. Unfortunately, this method is not feasible for large-scale production and hence limited to fundamental research applications only. Micromechanical cleavage is schematically represented in Fig. 5.2.

5.3.1.2 Solution and Thermal Exfoliation

Separation of few layers of graphene from 3D layered bulk graphite gains tremendous interest due to the increased electrical conductivity from 3D bulk scale to the 2D nanoscale. Hence, different exfoliation approaches have been demonstrated to produce graphene nanosheets. Initially, the mechanical exfoliation process uses HOPG (highly oriented pyrolytic graphite) as a precursor, subjected to an oxygen plasma etching to create 5- μm -deep mesas, and scotch tape was used to repeatedly peel graphite flakes from the mesas [12]. In addition, exfoliation of wet chemically derived graphite layers is another route for separation of individual sheets of graphene, mainly attractive for a large area sheet fabrication with a possible large volume of production [13–15]. The most common disadvantage of wet techniques is the formation of by-products, which contaminate the graphite layers. Hence, the

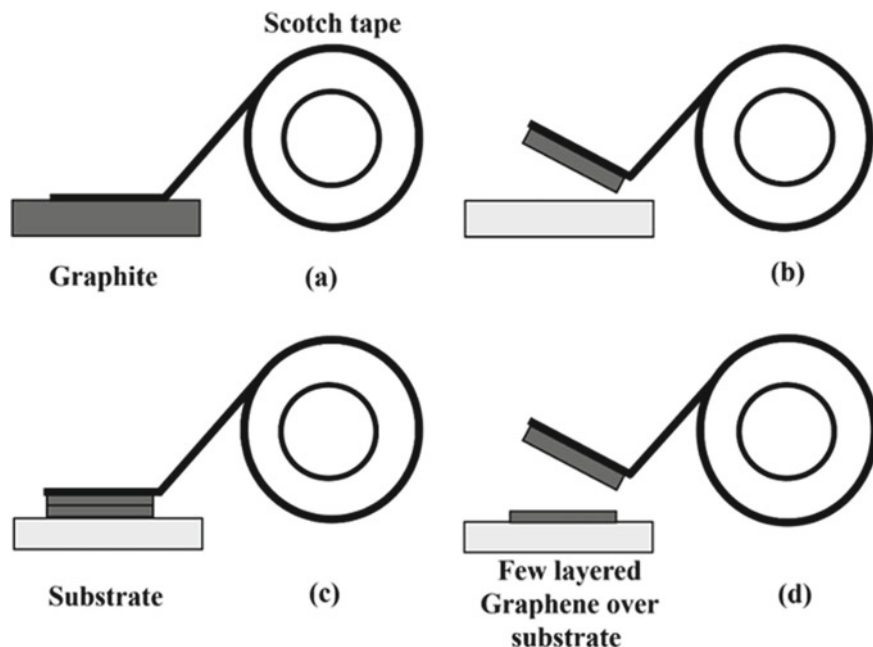


Fig. 5.2 Schematic representation of micromechanical cleavage technique, **a** and **b** adhesive tape is used to cleave the top few layers of bulk graphite, **c** graphitic tape pressed on desired substrate, **d** few layers remain on the substrate. Redrawn and reprinted with permission from [11]

development of a one-step procedure could yield in high per cent, cost-effective and efficient large-scale monolayer graphene. Several organic solvents have been studied so far to exfoliate graphene oxide (GO) assisted by thermal reduction as schematically represented in Fig. 5.3.

The most common solvent used for the reduction in GO is propylene carbonate (PC) due to excellent dispersion ability. This technique could lead to large-scale production of graphene in an easy one-step procedure [16]. In particular, the improvement of reduction in the presence of PC has been demonstrated employing the increase of ultrasonication time. Moreover, a liquid-phase exfoliation has been demonstrated to produce high quality and defect-free large-area graphene sheets upon treatment with N-methyl-2-pyrrolidone (NMP) operating at $\sim 800^\circ\text{C}$ [17]. Therefore, thermal treatments have been heavily used as the next step following wet-processing techniques for thin film preparation. In addition, microwave exfoliation has achieved great interest for thermal treatment. Microwave irradiation is an effective and attractive method for graphene synthesis with controllable size and shape as compared to conventional heating due to the homogeneous distribution of heat energy.

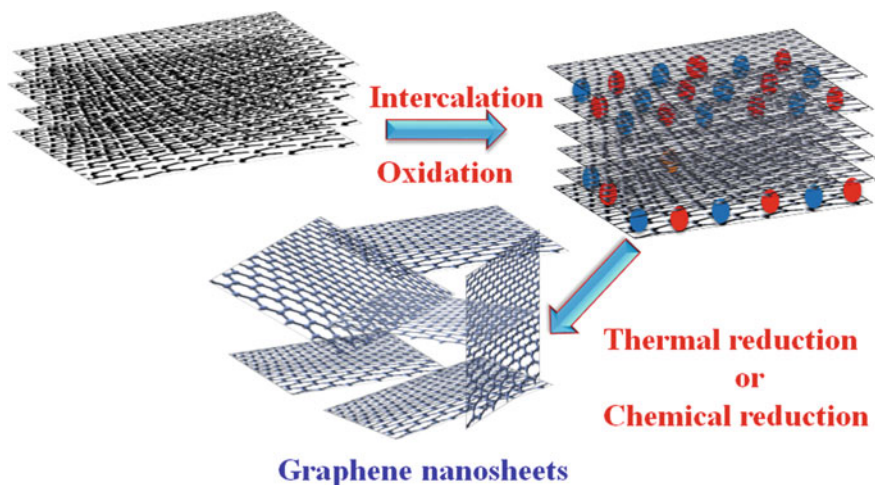


Fig. 5.3 Intercalation or exfoliation process for synthesis of graphene nanosheets. Drawn based on the concept taken from [15]

5.3.2 Chemical Vapour Deposition

Many methods have been reported for the production of graphene to date. Chemical vapour deposition (CVD) and its variants with transition metal substrates retain a great attention for large-area continuous film production and commercialization of graphene [18, 19]. CVD technique deposits solid thin film through the vapour or gases by chemical reactions on desire substrates. Figure 5.4 shows the schematic of a tube-furnace CVD instrument for the growth of graphene on the desire substrate. It is composed of a gas delivery system consisting of necessary valves, mass flow controllers, pressure controller that regulate the flow rates of the gases and a gas mixing unit, which is responsible for mixing of various gases uniformly before they are subjected to the reactor, a reactor and gas removal system. During the synthesis process, reactive gas species are fed into the reactor by the gas delivery system in which the chemical reaction takes place. The heater helps to achieve high temperature, and solid materials are uniformly deposited on the desire substrates.

The by-products of reaction and non-reacted gases are removed by the gas delivery system. Growth of graphene by CVD on polycrystalline metals such as Ir, Ni, Pt, Pd, Rh, Cu and Co has been thoroughly studied and investigated [20]. CVD processes have reported that graphene is obtained by nucleation of active carbon formed by the decomposition of precursor materials on the metal surface. The metal surface plays the role of an active catalyst material. Moreover, catalyst-free growth of graphene on Si, W, Mo, SiO₂ and Al₂O₃ has also been demonstrated by ECR-CVD and PECVD methods [21–24]. Furthermore, continuous defect-free graphene films at low temperature have been reported by MPCVD [25, 26]. Graphene film growth over polycrystalline Ni by CVD has primarily been performed at atmospheric pressure,

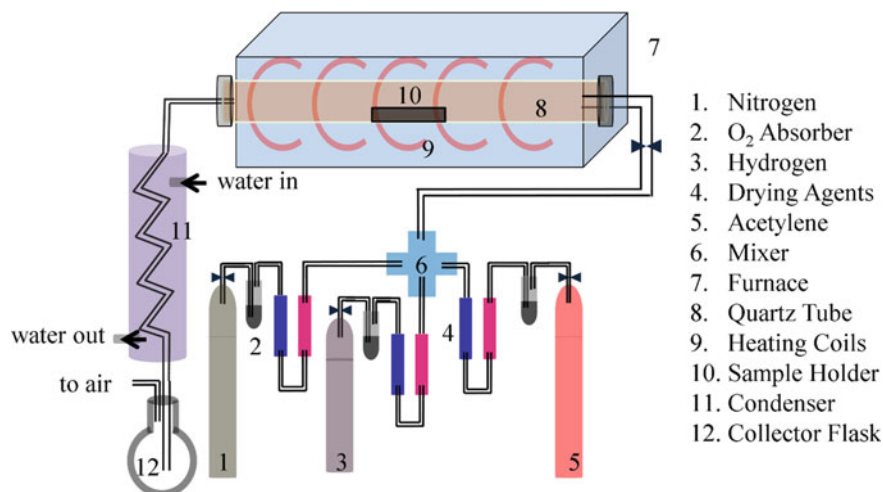


Fig. 5.4 Schematic illustration of chemical vapour deposition set-up

yielding graphene continuous films [26–28]. In contrast, annealing of the polycrystalline nickel [29] and an increase in deposition temperature [30] strongly promote the synthesis of large grain sizes of Ni (111) over Ni (100). Moreover, many reports have been published so far on the effect on synthesis parameters such as growth temperature, gas mixing ratio and growth time in the chemical vapour deposition of acetylene/hydrogen. These are the deciding parameters for producing few-layer graphene continuous film with minimal defects [26, 31].

In addition, the growth of few-layer graphene continuous film on nickel surface has also been fabricated based on diffusion and segregation phenomena of carbon from underlying amorphous carbon or nanodiamond films [32, 33]. Hence, bilayer graphene films have been fabricated directly on self-assembled monolayers (SAMs) or insulating substrates at low pressure [34]. In addition, few-layer continuous graphene film on SiO₂/Si from SAMs has been fabricated at atmospheric pressure and transfer-free graphene growth with uniform thickness has been achieved [35]. Meanwhile, a uniform and low-defect bilayer graphene has been synthesized on evaporated polycrystalline nickel films after exposing methane at 1000 °C with optimized process parameters such as growth time, annealing profile and flow rates of different gases. Raman mapping shows the ratio of 2D to G peak intensities (I_{2D}/I_G) is in the range of 0.9–1.6 over 96% of the 200 × 200 μm areas and the average ratio of D to G peak intensity (I_D/I_G) is about 0.1, confirms the bilayer formation [36].

Furthermore, the growth of graphene on several hexagonal surfaces has also been studied. Hexagonal substrates are frequently referred for growth of graphene due to the less lattice mismatch. Co (0001) and Ni (111) show less than 1% lattice mismatch [37, 38]. In contrast, the lattice mismatch between graphene and Pt (111) [39], Pd (111) [40], Ru (111) [41] and Ir (111) [42] is greater than 1%, and therefore, the growth is incommensurate. Recently, graphene growth on relatively polycrystalline

Ni [43, 44] and Cu [45] substrates has been triggered interest in fabrication and optimizing CVD conditions for large-area deposition and transfer. Moreover, copper has also been studied as a catalyst to grow several carbon allotropes such as graphite [46], diamond [47] and carbon nanotubes [48, 49].

The growth of graphene on copper is due to the surface and independent of diffusion from bulk. Based on earlier literature, a possible model for the nucleation and three-stages of growth mechanism of graphene on copper can be suggested. As the growth time is higher, the graphene domains increase. A facile technique for the growth of graphene directly on substrates through a simple thermal annealing process has been demonstrated [50]. Transparent graphene film has been prepared successfully and transferred by using a roll-to-roll transfer technique with the help of a thermal release tape as a support polymer. A large-area touch screen has been prepared with the graphene so transferred over the substrate. The thermal adhesive tape plays a key role in this transfer process of these very large-area graphene films from copper to plastic substrate materials [51].

5.3.3 *Graphene/Reduced Graphene Oxide from Graphene Oxide*

Large-scale production of graphene is a great challenge. One of the best cost-effective methods for mass production of graphene is the reduction of graphene oxide (GO) in the presence of a reducing agent. GO has been first prepared by Benjamin C. Brodie by repeatedly treating the graphite with potassium chlorate in the presence of nitric acid [52]. Later, the most commonly used and less hazardous method has been proposed by Hummers and Offeman, which involves the oxidation of graphite by treating graphite with a mixture of sulphuric acid, sodium nitrate and potassium permanganate. This is the most popular chemical route of graphene/reduced GO synthesis, nowadays. During oxidation of graphite, individual sheets of GO have been designed with oxygen-containing functional groups such as carbonyl, hydroxyl and epoxy on both sides of the plane as well as the edges [53]. Hence, GO exhibits negatively charged features and electrostatically stabilized in water, alcohols and certain organic solvents. The maximum lateral size of GO sheets is strongly dependent on the size of initial graphite crystals used for graphite oxidation. Due to nonstoichiometric composition, the determination of GO structure is a challenge and strongly depends on the synthetic methods. Generally, oxygen is present on the basal plane of GO in the form of hydroxyl, epoxy, carboxyl, carbonyl groups, etc. and is also located at the planar edges as shown in Fig. 5.5. Hence, GO exhibits electrical insulation and can produce homogeneous colloidal suspensions.

Therefore, to restore the electronic property of graphene, reduction (by chemical or thermal route) is required to remove the oxygen functional groups as shown in Fig. 5.6.

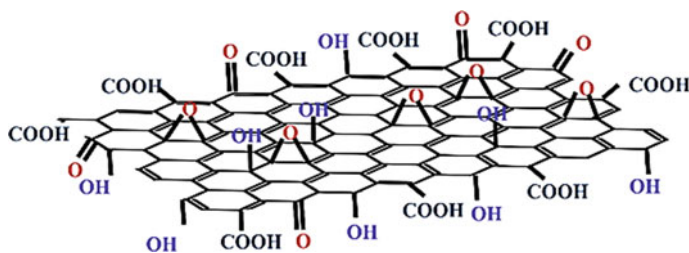


Fig. 5.5 Surface functional groups of graphene oxide. Redrawn and reprinted with permission from [54]

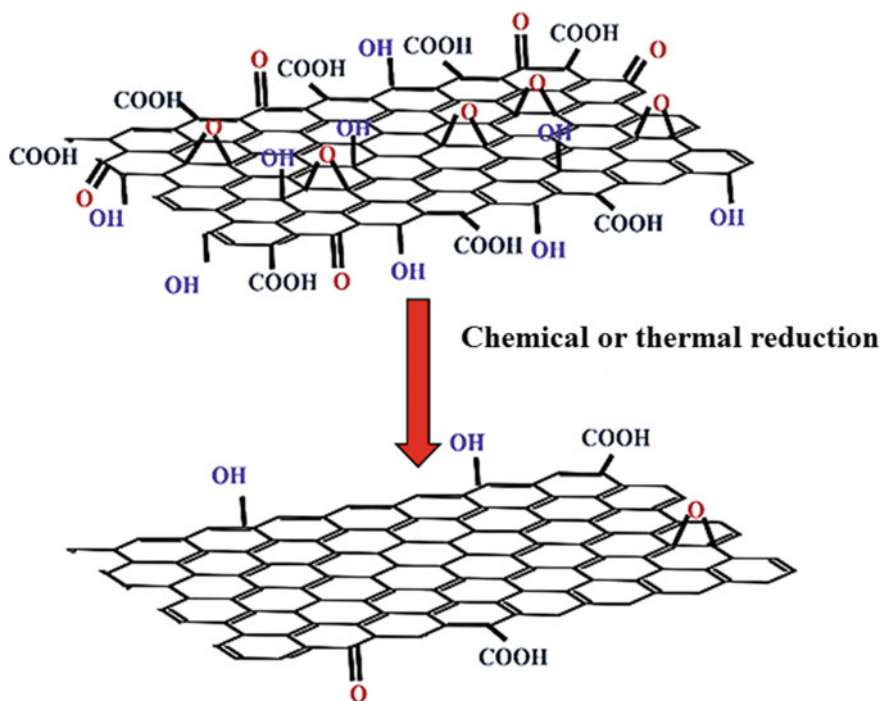


Fig. 5.6 Schematic illustration of reduction in graphene oxide into graphene sheet. Redrawn and reprinted with permission from [55]

5.3.3.1 Hazardous Approach of Graphene Oxide Reduction

During chemical reduction by reducing agent, the colour of GO dispersion (initially light yellow) in water turns into blackish colour and strongly suggests the removal of oxygen species. Generally, the chemical reduction in GO sheets has been performed with different reducing agents. For examples, these are hydrazine (N_2H_4) [56], sodium borohydride ($NaBH_4$) [57], hydriodic acid (HI) [58], hydroquinone

[59], etc. However, the chemical reduction in GO has many drawbacks such as chemical toxicity (these reducing agents not only toxic but also explosive in nature) and therefore hazardous to our environment. Hence, less toxic reducing agents such as metal nanoparticles [60], sulphuric acid (H_2SO_4) [61], sodium hypophosphite (Na_3PO_2) [62], bismuth ferrite (BiFeO_3) [63], aluminium iodide (AlI_3) [64] and phenolic acids have been studied as alternatives. However, such reducing agents imprint some amount of damaging chemical traces on the graphene surface and are not suitable enough for bio-related applications. Hence, the green approach of reduction comes into play.

5.3.3.2 Green Approach of Graphene Oxide Reduction

Developments and optimizations have been explored to reduce GO by eco-friendly techniques [65–67]. For example, Cote et al. have used a chemical-free room-temperature flash reduction process for the reduction in GO by photothermal heating using photographic camera flash [68]. Flash irradiation triggers the deoxygenation reaction of GO and rapidly creates a fused polymer composite. They have prepared composite patterns such as interdigitated electrode arrays by using photomask on flexible substrates [68]. Ghadim et al. have used nanosecond pulsed laser (having wavelength of 532 nm and average power of 0.3 W) for the effective and environment-friendly reduction in GO sheets in ammonia solution ($\text{pH} \sim 9$) at room temperature [69]. Based on X-ray photoelectron spectroscopy (XPS) analysis, the O/C ratio of the GO sheets decreases from 49 to 21% after 10 min of laser irradiation. These results help further promotion and application of pulsed lasers for the reduction in GO in environment-friendly way [69]. In addition, Zhou et al. have reported a simple, clean and controlled hydrothermal dehydration route to convert GO to a stable graphene solution [70]. Compared to chemical reduction processes using hydrazine, the present ‘water-only’ route has the combined advantages of removing oxygen-containing functional groups from GO and fixing the aromatic structures for tunable optical limiting performance [70]. Moreover, Ai et al. have adopted a simplistic and efficient way for the preparation of soluble reduced graphene oxide (rGO) sheets [71]. In this process, reduction in GO has been done by reducing agent, dimethylformamide (DMF). The as-prepared rGO sheets exhibit a high reduction level, good conductivity, and are well dispersed in many solvents. Synthesized rGO sheets show potential applications in the construction of high-performance graphene-based NO gas sensing devices [71]. Xu et al. have adopted a simple approach for the preparation of graphene–metal particle nanocomposites in a water–ethylene glycol system [72]. GO is used as a precursor and metal nanoparticles (Au, Pt and Pd) as building blocks. The nanoparticles adsorb on GO sheets and play a vital role in catalytic reduction in GO. Cyclic voltammogram analyses have indicated its potential application in direct methanol fuel cells [72]. Consequently, Akhavan et al. have synthesized GO platelets by using a chemical exfoliation method to deposit anatase TiO_2 thin films [73]. Post-annealing of the GO/ TiO_2 thin films at 400 °C in air partially produces Ti–C bond between the platelets. The annealed GO/ TiO_2 thin films are immersed in

ethanol, and photocatalytic reduction has commenced. After 4 h of photocatalytic reduction, the concentration of the C=O bond has been reduced to 85%, indicating the effective reduction in the GO platelets to graphene nanosheets. The GO/TiO₂ thin film has been utilized as nanocomposite photocatalysts for the degradation of E. coli in an aqueous solution under solar light irradiation [73]. Consequently, biological approaches have been used to synthesized rGO from GO. For example, vitamin C [74], sugar [75], glucose [76], bovine serum albumin [77], melatonin [78], green tea [79], ginseng [80], curcumin [81], bacteria [82] and bacteriorhodopsin [83] have been explored in the literature. Hence, green methodologies are promising for the reduction in GO with a minimized environmental impact.

5.4 Properties of Graphene

5.4.1 Electronic Properties

Graphene has excellent structural flexibility that is well reflected in electrical properties of it [84]. The sp² hybridization between *s* and *p* orbitals generates a trigonal planar structure leading to the formation of a σ bond between the carbon atoms separated by 1.42 Å. The σ bands in graphene provide the structural robustness in graphene. These bands retain a filled shell and form deep valence bands. The *p* orbitals, which are unaffected, remain perpendicular to the planar structure. This helps in the formation of covalent bonds with the neighbouring carbon atoms generating π bands. The *p* orbitals have one extra electron showing the half-filled configuration. The half-filled configuration plays a crucial role in determining the physics behind the system. The tight-binding character in graphene leads to large Coulomb energies, which in turn show strong collective effects such as magnetism and insulating behavior as a result of correlation gaps [85]. Linus Pauling proposes that the electronic properties of graphene are on the basis of resonant valence bond (RVB) structure. However, this theoretical understanding of electronic properties of graphene if compared with the band structure of graphene, it is found to play a role of a semimetal with Dirac electrons. Here, it is worthy to mention, most of the current experimental studies on the electronic properties of graphene are based on its band structure. However, the electron–electron interaction in graphene is a matter of intense research.

The energy dispersion of graphene was formulated, and tight-binding Hamiltonian was described to explain electrons in graphene [86]. By using tight-binding Hamiltonian, the energy dispersion relation has been represented as [87]:

$$E^{\pm}(k_x, k_y) = \pm\gamma_0\sqrt{1 + 4\cos\frac{\sqrt{3}k_x a}{2}\cos\frac{k_y a}{2} + 4\cos^2\frac{k_y a}{2}} \quad (5.6)$$

where γ_0 is the first-neighbour π -orbitals energy (2.9 – 3.1 eV), $a \sim 1.42 \text{ \AA}$ is the lattice constant and $k = (k_x, k_y)$ vectors denote the first Brillouin zone electronic momenta.

This energy dispersion will have six points, where the conduction and valence band touch each other called Dirac points. The ballistic transport at this point with a mean free path of 300–500 nm takes place as shown in Fig. 5.7. This makes graphene a semi-metal. The linear dispersion near the Dirac points will then be:

$$E_{\pm}(\mathbf{k}) = \pm \hbar v_F |k| \quad (5.7)$$

Here, \hbar is the reduced Planck constant and v_F is the Fermi velocity ($\sim 10^6 \text{ m/s}$) [10, 87].

Mobility of graphene has been reported between 2000 and 20,000 $\text{cm}^2 \text{ V}^{-1} \text{ s}^{-1}$ on different substrates at low temperatures and carrier concentrations in the order of 10^{12} cm^{-2} [89]. Moreover, the suspended single-layer graphene shows mobility over 200,000 $\text{cm}^2 \text{ V}^{-1} \text{ s}^{-1}$ at electron densities of $\sim 2 \times 10^{11} \text{ cm}^{-2}$. This result is found when single-layer graphene suspension ($\sim 150 \text{ nm}$) has been deposited over a Si/SiO₂ gate electrode by electron beam lithography. Significant enhancement in the mobility has been achieved and widths of the characteristic Dirac peaks have been reduced by a factor of 10 compared to non-suspended devices [90]. Meanwhile, the Drude model assumes that the conductivity of graphene is in the range from 0.0032 to 0.00032 S in unsuspended graphene and the order of 0.0032 S for suspended graphene. The theoretical value of minimal conductivity is in the order of $e^2/h\pi$. However, in practice, the minimal conductivity has been achieved π times larger than the value of e^2/h [1, 91].

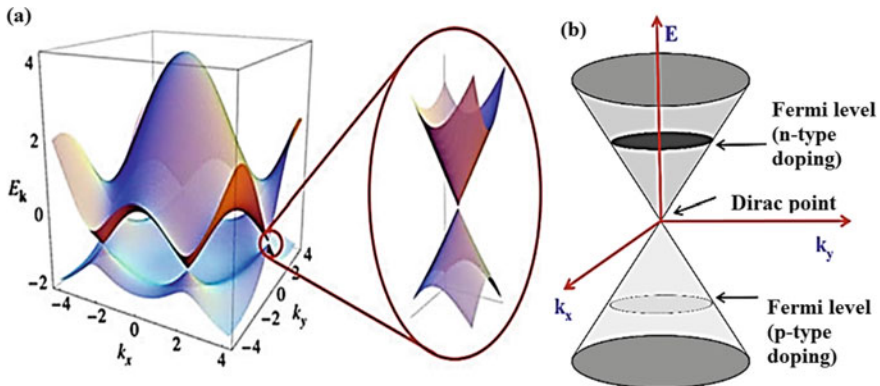


Fig. 5.7 a Graphene band structure as two cones touching at Dirac point. Reprinted with permission from [10] and b the position of the Fermi level determining nature of doping and transport carrier (redrawn and reprinted with permission from [88])

5.4.2 Optical Properties

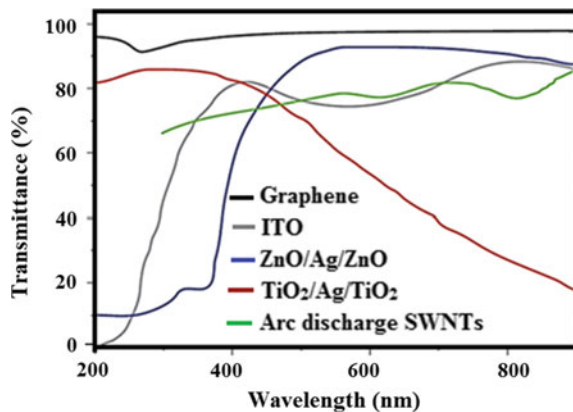
Monolayer graphene has shown 97.7% of light transmittance [92]. The absorption of the graphene depends on the fine-structure constant (α) and increases linearly with the number of layers of graphene stacked together (experimentally demonstrated up to five layers). Fresnel equation has been applied with a universal optical conductance ($G_0 = e^2/4\hbar \approx 6.08 \times 10^{-5} \Omega^{-1}$) to give the absorbance of freestanding monolayer graphene [87]:

$$T = (1 + 0.5\pi\alpha)^{-2} \approx 1 - \pi\alpha \approx 97.7\% \quad (5.8)$$

where $\alpha (= e^2/(4\pi\epsilon_0\hbar c) = G_0/(\pi\epsilon_0 c) \approx 1/137)$ is fine-structure constant. Graphene reflects <0.1% of the incident light in the visible region, rising to ~2% for ten layers. Hence, we can take the optical absorption of graphene to be proportional to the number of layers, each absorbing $A \approx 1 - T \approx \pi\alpha \approx 2.3\%$ over the visible spectrum. The absorption spectrum of monolayer graphene gives a peak at 270 nm in the ultraviolet region due to the exciton-shifted Van Hove singularity in the graphene density of states. In few-layered graphene, interband transitions at lower energies can be seen. Figure 5.8 gives an overview of different transparent conductors including single-walled carbon nanotubes (SWNTs), ITO, ZnO/Ag/ZnO and TiO₂/Ag/TiO₂ and graphene with their transmittance. It is evident that the transmittance for SWNTs ~ 70–80%, ITO ~ 70–90%, ZnO/Ag/ZnO ~ 90%, TiO₂/Ag/TiO₂ ~ 60–70% and for graphene ~ 95% have been achieved. Among these transparent conductors, graphene has higher transmittance over a wider range of wavelengths [87].

The optical transition in graphene has been measured by infrared spectroscopy, and the study reveals that the optical transition is gate dependent [93]. Near the Dirac point of a graphene sheet, the density of states remain low. Hence, a change of Fermi level owing to gate leads to variation in charge density to a great extent followed by

Fig. 5.8 Transmittance of graphene compared to that of other materials. Redrawn and reprinted with permission from [87]



modified transition characteristics. The process of relaxation and recombination of electron and hole pairs in graphene have been governed by the carrier concentration and are noticed on a timescale of tens of picoseconds [94, 95]. Graphene can be extensively used in high-speed optoelectronics due to the remarkable carrier transport velocity under electric field [96].

5.4.3 Thermal Properties

Heat removal in the electronic industry has become a crucial issue. Therefore, a rapid growth of interest has been seen in the thermal properties of material by the scientific communities around the globe. A variety of carbon allotropes having different thermal conductivity have been studied and occupy a unique place in particular applications. Thermal conductivity of different carbon materials has been found from $0.01 \text{ W m}^{-1} \text{ K}^{-1}$ in amorphous carbon to above $2000 \text{ W m}^{-1} \text{ K}^{-1}$ in diamond at room temperature or one-atom-thick 2D graphene as shown in Fig. 5.9 [97]. An interesting fact can be noticed by evaluating the thermal conductivities of few layers of graphene as a function of layer thickness or number of atomic planes. Here, the transport phenomena are restricted by two properties, one intrinsic and other extrinsic. The extrinsic properties of few-layer graphene are dependent on the defect scattering. The increase in the atomic plane of graphene leads to a major change in

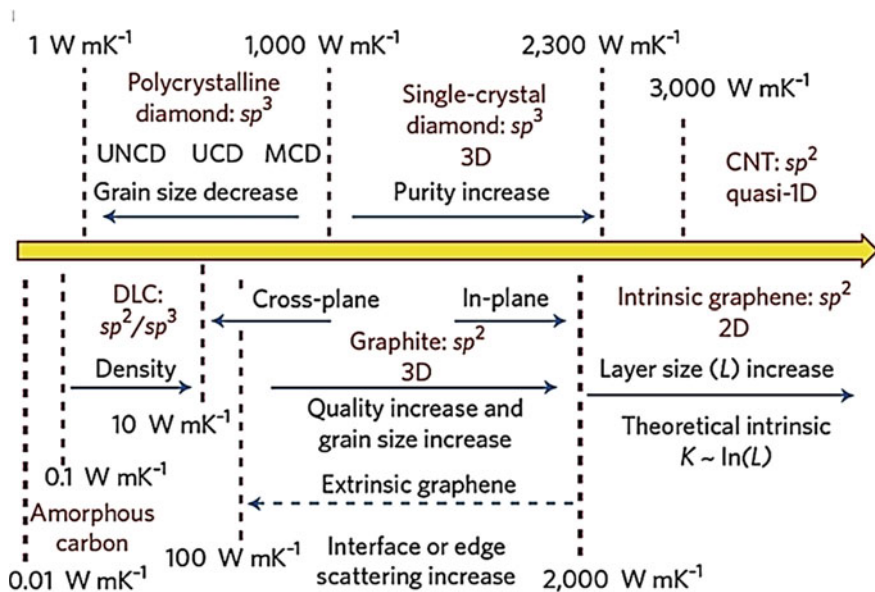


Fig. 5.9 Thermal conductivity of carbon allotropes and their derivatives. Reprinted with permission from [97]

phonon dispersion, and more and more phase space is obtainable for scattering to proceed. Hence, the scattering of phonon from top to bottom boundaries has been restricted if the constant number of atomic planes is maintained over the entire length of graphene layer [98].

The thermal conductivity of graphene has been measured first using Raman optothermal techniques in non-contact mode [5, 97]. The measurements are carried out with suspended graphene layers obtained by exfoliation of bulk graphite. This method of determination is essential to obtain the thermal conductivity of atomically thin graphene. Results report that thermal conductivity may exceed $3000 \text{ W m}^{-1} \text{ K}^{-1}$ at room temperature for large flakes of graphene [98]. The thermal conductivity values of graphene are reported to be better than bulk graphite in this study. The room-temperature thermal conductivity of CNTs has been found $3000\text{--}3500 \text{ W m}^{-1} \text{ K}^{-1}$. The suspended single-layer graphene has shown thermal conductivity in the range of $4.84 \pm 0.44 \times 10^3$ to $5.30 \pm 0.48 \times 10^3 \text{ W m}^{-1} \text{ K}^{-1}$ [99]. The thermal conductivity of non-doped graphene is not very much dependant on electronic contribution due to low carrier concentration. The thermal conductivity, in this case, is governed by phonon transport specifically termed as diffusive and ballistic conduction at high and low temperatures, respectively [100]. Molecular dynamic simulation study reveals the relation as $\kappa \propto 1/T$ for pure graphene $>100 \text{ K}$. At room temperature, $6000 \text{ W m}^{-1} \text{ K}^{-1}$ has been predicted, which is quite high compared to graphitic carbon under the same condition [101]. In another work, the thermal conductivity of single-layer graphene flakes obtained by exfoliation is calculated to be around $5000 \text{ W m}^{-1} \text{ K}^{-1}$ [102]. Graphene is suspended in a channel, and laser beam is focused from the center to support. The loss of heat through the air is nominal compared to the conduction of heat in graphene [103]. In this study, the frequency of Raman G peak is calculated in terms of laser excitation power. The thermal conductivity of the graphene has been evaluated from the slope of the trend line. These values are remarkably good and suggest that graphene is a very good material from a thermal point of view. Thermal conductivity of graphene can be tuned to a wide range by the introduction of disorder or edge roughness into the honeycomb lattice. Hence, the excellent heat-conduction properties of graphene make it a promising candidate for all proposed electronic and photonic applications.

5.4.4 Mechanical Properties

Inherent strength makes graphene so special. It is not only extraordinary strong ($E = 1.0 \text{ TPa}$) but also light in weight (0.77 mg m^{-2}) [1]. The elastic properties and intrinsic breaking strength of monolayer graphene have been measured by nanoindentation in an atomic force microscope. Using an atomic force microscope, effective spring constants have been measured for stacks of graphene sheets (less than 5 with sheets of thicknesses between 2 and 8 nm) suspended over photolithographically defined trenches in SiO_2 (schematically shown in Fig. 5.10). Graphene shows nonlinear elastic stress-strain response, yields second-order elastic stiffness of 340 N m^{-1}

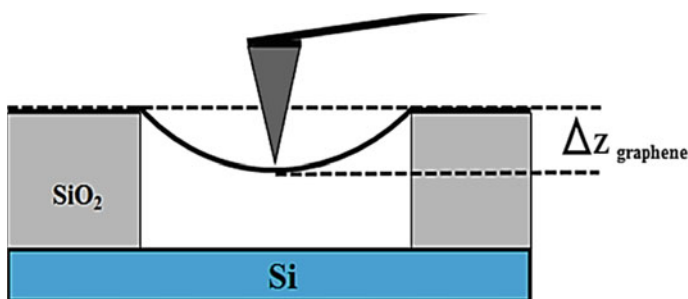


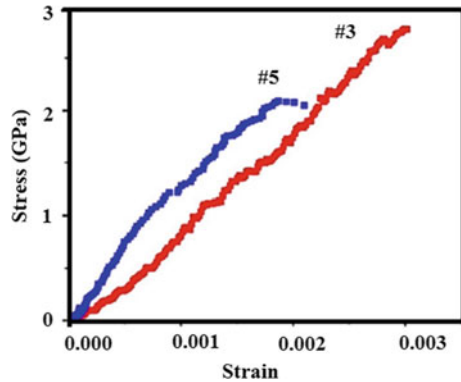
Fig. 5.10 Schematic illustration of AFM tip pushing down a suspended graphene sheet. Redrawn and reprinted with permission from [104]

and third-order elastic stiffness of 690 N m^{-1} . In addition, the breaking strength is found 42 N m^{-1} and Young's modulus of $E = 1.0 \text{ TPa}$. These experiments establish graphene as the strongest material ever measured [104].

The mechanical properties of single-layer graphene have been studied by numerical simulations, i.e. molecular dynamics [105–107]. AFM has also been used for a circular membrane of few-layer graphene by force–volume measurements [108]. Determination of mechanical properties of graphene by AFM studies is commonly carried out by indentation method [109]. A mean elastic modulus of 0.25 TPa has been reported in this measurement for chemically modified graphene. Study also remains, where the mechanical properties of graphene oxide platelets have been determined by fabricating paper-like material [110]. The results report a fracture strength and elastic modulus of $<120 \text{ MPa}$ and $<32 \text{ GPa}$, respectively. The improvement in mechanical performance of these paper-like materials has been evidenced due to the chemical crosslinking between individual platelets with divalent ions and polyallylamine [111, 112].

The excellent mechanical properties of graphene broaden up its application both as individual and reinforcing materials for the preparation of composites. The exceptionally good mechanical properties of graphene are due to the stable sp^2 bonds that face the in-plane deformations. Nicholl et al. demonstrate a non-contact experimental approach using interferometric profilometry [113, 114]. In this approach, both CVD and exfoliated graphene have been subjected to pressurize by electrostatic way through the application of a voltage between the membrane and gating chip. The study reveals that graphene exhibits in-plane stiffness of $20\text{--}100 \text{ N m}^{-1}$ at room temperature and has been softened considerably due to the out-of-plane crumpling effect. The defect-free single layer of graphene is considered to be the strongest material since others have studied the intrinsic strength of graphene membrane of 42 N m^{-1} , which equates to 130 GPa [7]. The effect of defects in graphene on intrinsic strength and stiffness has also been explored [114, 115]. In this study, the defects are introduced by modified plasma methods with AFM nanoindentation technique to subsequently measure the stiffness and strength of defective graphene. The defects are of sp^3 type and vacancy dominated determined from I_D/I_{D0} ratio of Raman peaks.

Fig. 5.11 Strain–strain curves for cracked graphene at different crack sizes; #3: 518 nm and #5: 1256 nm. Reprinted with permission from [117]



The quantification of defects is also done based on Raman studies by considering the ratio of I_D/I_G and I_{2D}/I_G ratios.

Interlayer shear mechanical properties of a multilayer graphene in wrinkled form have been predicted by simulation [116]. Results show that the mechanical properties of the wrinkled graphene have been improved compared to flat counterpart due to favourable geometrical locking. Graphene layers of different aspect ratios have been chosen. The shape of the wrinkled sheet remains unaltered when the aspect ratio is 0.77, and however, a change in the interlayer distance has been evidenced. The geometrical locking in the structure prevents the flipping over the deformation, and hence, the separation between two layers of the graphene takes place, which leads to a change in its interlayer distance. The wrinkled graphene is expected to reach tensile strength of 12 GPa due to interlayer shear modulus and strength. Determination of fracture toughness is another important mechanical properties of graphene that is relevant to engineering application. An in situ micromechanical testing device has been developed by Zhang et al. [117]. The fracture toughness of graphene synthesized in CVD mode has been determined by using a nanoindenter clubbed with scanning electron microscopy. A central crack has been induced using the focused ion beam, and brittle fracture has been noticed once the load is applied. The fracture stress is found to be increased with crack length. The critical strain release rate attained in this study is 15.9 J m^{-2} , and a fracture toughness of about 4 MPa has been reported. Figure 5.11 displays the engineering stress–strain curves for cracked graphene for crack sizes of 518 and 1256 nm.

5.5 Doping of Hetero-atoms into Graphene Lattice

Chemical doping is an efficient process, which provides the opportunity to tailor the electronic, chemical, optical and magnetic properties of materials [118, 119]. Graphene doped with different atoms (i.e. boron (B), nitrogen (N), sulphur (S), silicon (Si), etc.) results change in electronic properties and chemical reactivity of

honeycomb lattice [120–123]. In particular, N-doping in graphene lattice produces additional *n*-type carriers for applications in high-frequency semiconductor devices and also enhances catalysis for energy conversion and storage [124–126]. In addition, N-doping shows biocompatibility and therefore is favourable for biosensing applications [127–129]. Recently, the highly crystalline monolayer N-doped graphene nanosheets have been synthesized and composed of two quasi-adjacent substitutional nitrogen atoms within the same graphene sub-lattice (N_2^A) with improved Raman scattering [130]. In addition, magnetic properties for foreign atoms such as B-atoms, S-atoms and F-atoms have been studied. Especially, B-doped graphene with strong electron-withdrawing capability has been studied, which gives a catalyst-free thermal annealing approach in the presence of boron oxide for oxygen reduction in fuel cell application [131]. B-atoms of ~3.2 at.% have been successfully doped into graphene lattice [131]. Furthermore, S-doped graphene has been studied by magnesiothermic reduction in easily available, low-cost, non-toxic CO_2 (obtained from Na_2CO_3 and Na_2SO_4) as carbon and sulphur sources for the synthesis of efficient metal-free electrocatalysts for oxygen reduction reaction (ORR). The S-doped graphene exhibits high activity for ORR with a four-electron pathway having superior durability and tolerance to methanol crossover to 40% [132].

5.6 Applications

The area of application of graphene is broad and diverse in true sense. Graphene grabs different field of application in recent years due to the promising properties as discussed earlier. In the field of medicine, graphene has been extensively researched by scientists and shows its potential in drug delivery, tissue engineering, bio-imaging, biomicrobiotics, etc. Graphene extends its applicability in modern energy devices both in the field of generation and storage [133]. Graphene is suitable to be used as transistors, transparent conducting electrodes, spintronics, conductive ink, quantum dots, electronic devices and many more due to amazing electronic properties [134]. Graphene has also been used as lubricants, structural materials, waterproof coating, catalysts, metamaterials, plasmonics and many more indicating its capability to be suitable in the wide area of applications. The unique band structure of graphene makes the charge carrier bipolar in nature that can be effectively tuned by the application of electric field [12]. Hence, graphene has been successfully investigated by various research groups as field-effect transistors [91, 135]. The field-effect mobility of graphene is about an order of magnitude higher than silicon. Monolayer graphene is an excellent material to detect different gases and biomolecules and has been studied extensively as sensors [136–139]. The charge transfer between graphene and adsorbed molecules is accountable for chemical response. When a molecule gets adsorbed on the surface of graphene, the location experiences a charge transfer. This leads to a change in Fermi level and electronic resistance of graphene. Graphene and graphene-based fillers have been widely used for the preparation of

polymer nanocomposites for possible use in wide application areas [140–142]. Polymer matrices of interest for the preparation of polymer nanocomposites with graphene are polystyrene, polyvinyl alcohol, polyester, epoxy, polycarbonate, polypropylene and many more [143–147].

5.7 Concluding Remarks

Graphene is a unique material in true sense. It is a material of choice for the modern day, a truly two-dimensional carbon material. Graphene has rare electronic excitation that moves in a curved space and interesting combinations of semiconductor and metal with the additional benefit of properties of a soft material. Graphene has different properties than conventional metal and semiconductors due to unusual electronic properties. The electron therein is undisturbed by the presence of disorder with a very long mean free path. Graphene has a robust but flexible structural arrangement. The properties of a graphene sheet can be modified by changing the number of layers, controlling the geometry, chemical doping and application of electric and magnetic field, etc. This chapter discusses the structure, synthesis and properties of graphene/reduced graphene oxide in detail. Graphene owing to its unique properties is found applications in different fields from chemical sensors to transistors. The application window of this material can be widened by chemical or structural modification of graphene to alter its functionality. Moreover, graphene can be easily synthesized from graphite, which is quite abundant on earth. This extends the availability of raw material for graphene synthesis for extensive research in this field.

Acknowledgements The authors acknowledge the financial support provided by Department of Science and Technology, India (DST/TMD/MES/2K16/37(G)), for carrying out this research work. Authors are thankful to Ms Tanvi Pal for drafting a figure.

References

1. A.K. Geim, K.S. Novoselov, *Nat. Mater.* **6**, 183 (2007)
2. S.P. Lonkar, Y.S. Deshmukh, A.A. Abdala, *Nano Res.* **8**, 1039 (2015)
3. S. Banerjee, P. Benjwal, M. Singh, K.K. Kar, *Appl. Surf. Sci.* **439**, 560 (2018)
4. R. Kumar, E.T. da Silva, R.K. Singh, R. Savu, A.V. Alaferdov, L.C. Fonseca, L.C. Carossi, A. Singh, S. Khandka, K.K. Kar, *J. Colloid Interface Sci.* **515**, 160 (2018)
5. A.A. Balandin, S. Ghosh, W. Bao, I. Calizo, D. Teweldebrhan, F. Miao, C.N. Lau, *Nano Lett.* **8**, 902 (2008)
6. W. Cai, Y. Zhu, X. Li, R.D. Piner, R.S. Ruoff, *Appl. Phys. Lett.* **95**, 123115 (2009)
7. C. Lee, X. Wei, J.W. Kysar, J. Hone, *Science* **321**, 385 (2008)
8. X. Li, Y. Zhu, W. Cai, M. Borysiak, B. Han, D. Chen, R.D. Piner, L. Colombo, R.S. Ruoff, *Nano Lett.* **9**, 4359 (2009)

9. H. O. Pierson, *Handbook of carbon, graphite, diamonds and fullerenes: Processing, properties and applications* (William Andrew, 2012)
10. A.C. Neto, F. Guinea, N.M. Peres, K.S. Novoselov, A.K. Geim, *Rev. Mod. Phys.* **81**, 109 (2009)
11. K. S. Novoselov, A. H. Castro Neto, *Phys. Scr.* **2012**, 014006 (2012)
12. K.S. Novoselov, A.K. Geim, S.V. Morozov, D. Jiang, Y. Zhang, S.V. Dubonos, I.V. Grigorieva, A.A. Firsov, *Science* **306**, 666 (2004)
13. A. Ciesielski, P. Samorì, *Chem. Soc. Rev.* **43**, 381 (2014)
14. M. Acik, Y.J. Chaba, *J. Mater. Sci. Res.* **2**, 101 (2013)
15. <https://www.princeton.edu/~cml/html/research/TEGO.html>. Accessed 10 January 2019
16. Y. Zhu, M.D. Stoller, W. Cai, A. Velamakanni, R.D. Piner, D. Chen, R.S. Ruoff, *ACS Nano* **4**, 1227 (2010)
17. S.Y. Oh, S.H. Kim, Y.S. Chi, T.J. Kang, *Appl. Surf. Sci.* **258**, 8837 (2012)
18. W. Choi, I. Lahiri, R. Seelaboyina, Y.S. Kang, *Crit. Rev. Solid State Mater. Sci.* **35**, 52 (2010)
19. <http://majalah1000guru.net/2013/05/carbon-nanotubes-material-cerdas/>. Accessed 10 January 2019
20. M. Batzill, *Surf. Sci. Rep.* **67**, 83 (2012)
21. H. Medina, Y.C. Lin, C. Jin, C.C. Lu, C.H. Yeh, K.P. Huang, K. Suenaga, J. Robertson, P.W. Chiu, *Adv. Funct. Mater.* **22**, 2123 (2012)
22. H.J. Song, M. Son, C. Park, H. Lim, M.P. Levendorf, A.W. Tsen, J. Park, H.C. Choi, *Nanoscale* **4**, 3050 (2012)
23. T. Takami, S. Ogawa, H. Sumi, T. Kaga, A. Saikubo, E. Ikenaga, M. Sato, M. Nihei, Y. Takakuwa, *e-J. Surf. Sci. Nanotechnol.* **7**, 882 (2009)
24. Y. Wang, X. Xu, J. Lu, M. Lin, Q. Bao, B. Ozyilmaz, K.P. Loh, *ACS Nano* **4**, 6146 (2010)
25. Y. Kim, W. Song, S. Lee, C. Jeon, W. Jung, M. Kim, C.-Y. Park, *Appl. Phys. Lett.* **98**, 263106 (2011)
26. R.S. Edwards, K.S. Coleman, *Acc. Chem. Res.* **46**, 23 (2013)
27. L. Gomez De Arco, Y. Zhang, C.W. Schlenker, K. Ryu, M.E. Thompson, C. Zhou, *ACS Nano* **4**, 2865 (2010)
28. A. Reina, X. Jia, J. Ho, D. Nezich, H. Son, V. Bulovic, M.S. Dresselhaus, J. Kong, *Nano Lett.* **9**, 30 (2008)
29. Y. Zhang, L. Gomez, F.N. Ishikawa, A. Madaria, K. Ryu, C. Wang, A. Badmaev, C. Zhou, *J. Phys. Chem. Lett.* **1**, 3101 (2010)
30. S. Thiele, A. Reina, P. Healey, J. Kedzierski, P. Wyatt, P.-L. Hsu, C. Keast, J. Schaefer, J. Kong, *Nanotechnol.* **21**, 015601 (2009)
31. S.J. Chae, F. Güneş, K.K. Kim, E.S. Kim, G.H. Han, S.M. Kim, H.J. Shin, S.M. Yoon, J.Y. Choi, M.H. Park, *Adv. Mater.* **21**, 2328 (2009)
32. J.M. Garcia, R. He, M.P. Jiang, P. Kim, L.N. Pfeiffer, A. Pinczuk, *Carbon* **49**, 1006 (2011)
33. M. Zheng, K. Takei, B. Hsia, H. Fang, X. Zhang, N. Ferralis, H. Ko, Y.-L. Chueh, Y. Zhang, R. Maboudian, *Appl. Phys. Lett.* **96**, 063110 (2010)
34. Z. Yan, Z. Peng, Z. Sun, J. Yao, Y. Zhu, Z. Liu, P.M. Ajayan, J.M. Tour, *ACS Nano* **5**, 8187 (2011)
35. H.J. Shin, W.M. Choi, S.M. Yoon, G.H. Han, Y.S. Woo, E.S. Kim, S.J. Chae, X.S. Li, A. Benayad, D.D. Loc, *Adv. Mater.* **23**, 4392 (2011)
36. A. Umair, H. Raza, *Nanoscale Res. Lett.* **7**, 437 (2012)
37. Y. Bando, Y. Takahashi, E. Ueta, N. Todoroki, T. Wadayama, *J. Electrochem. Soc.* **162**, F463 (2015)
38. J. Hamilton, J. Blakely, *Surf. Sci.* **91**, 199 (1980)
39. P. Sutter, J.T. Sadowski, E. Sutter, *Phys. Rev. B* **80**, 245411 (2009)
40. S.-Y. Kwon, C.V. Ciobanu, V. Petrova, V.B. Shenoy, J. Bareno, V. Gambin, I. Petrov, S. Kodambaka, *Nano Lett.* **9**, 3985 (2009)
41. P.W. Sutter, J.-I. Flege, E.A. Sutter, *Nat. Mater.* **7**, 406 (2008)
42. J. Coraux, M. Engler, C. Busse, D. Wall, N. Buckanie, F.-J. M. Zu Heringdorf, R. Van Gastel, B. Poelsema, T. Michely, *New J. Phys.* **11**, 023006 (2009)

43. Z.-Y. Juang, C.-Y. Wu, A.-Y. Lu, C.-Y. Su, K.-C. Leou, F.-R. Chen, C.-H. Tsai, *Carbon* **48**, 3169 (2010)
44. H.J. Park, J. Meyer, S. Roth, V. Skákalová, *Carbon* **48**, 1088 (2010)
45. X. Li, L. Colombo, R.S. Ruoff, *Adv. Mater.* **28**, 6247 (2016)
46. O. Carneiro, M. Kim, J. Yim, N. Rodriguez, R. Baker, *J. Phys. Chem. B* **107**, 4237 (2003)
47. L. Constant, C. Speisser, F. Le Normand, *Surf. Sci.* **387**, 28 (1997)
48. L. Ding, A. Tselev, J. Wang, D. Yuan, H. Chu, T.P. McNicholas, Y. Li, J. Liu, *Nano Lett.* **9**, 800 (2009)
49. W. Zhou, Z. Han, J. Wang, Y. Zhang, Z. Jin, X. Sun, Y. Zhang, C. Yan, Y. Li, *Nano Lett.* **6**, 2987 (2006)
50. C. Jia, J. Jiang, L. Gan, X. Guo, *Sci. Rep.* **2**, 707 (2012)
51. S. Bae, H. Kim, Y. Lee, X. Xu, J.-S. Park, Y. Zheng, J. Balakrishnan, T. Lei, H.R. Kim, Y.I. Song, *Nat. Nanotechnol.* **5**, 574 (2010)
52. M. Aliofkhazraei, N. Ali, W. I. Milne, C. S. Ozkan, S. Mitura, J. L. Gervasoni, *Graphene science handbook: Fabrication methods* (CRC Press, 2016)
53. D. Lee, L. De Los Santos V, J. Seo, L. L. Felix, A. Bustamante D, J. Cole, C. Barnes, *J. Phys. Chem. B* **114**, 5723 (2010)
54. O.C. Compton, S.T. Nguyen, *Small* **6**, 711 (2010)
55. H. Li, C. Bubeck, *Macromol. Research* **21**, 290 (2013)
56. S. Park, R.S. Ruoff, *Nat. Nanotechnol.* **4**, 217 (2009)
57. H.J. Shin, K.K. Kim, A. Benayad, S.M. Yoon, H.K. Park, I.S. Jung, M.H. Jin, H.K. Jeong, J.M. Kim, J.Y. Choi, *Adv. Funct. Mater.* **19**, 1987 (2009)
58. I.K. Moon, J. Lee, R.S. Ruoff, H. Lee, *Nat. Commun.* **1**, 73 (2010)
59. C. Li, L. Li, L. Sun, Z. Pei, J. Xie, S. Zhang, *Carbon* **89**, 74 (2015)
60. P. Labhane, L. Patle, V. Huse, G. Sonawane, S. Sonawane, *Chem. Phys. Lett.* **661**, 13 (2016)
61. Y. Hong, Z. Wang, X. Jin, *Sci. Rep.* **3**, 3439 (2013)
62. C. Liu, G. Han, Y. Chang, Y. Xiao, Y. Li, M. Li, H. Zhou, *Chin. J. Chem.* **34**, 89 (2016)
63. Z.-T. Hu, J. Liu, X. Yan, W.-D. Oh, T.-T. Lim, *Chem. Eng. J.* **262**, 1022 (2015)
64. C. Liu, F. Hao, X. Zhao, Q. Zhao, S. Luo, H. Lin, *Sci. Rep.* **4**, 3965 (2014)
65. M. Aunkor, I. Mahbulul, R. Saidur, H. Metselaar, *Rsc Adv.* **6**, 27807 (2016)
66. P. Chamoli, M.K. Das, K.K. Kar, *Curr. Graphene Sci.* **1**, 000 (2017)
67. P. Chamoli, M.K. Das, K.K. Kar, *J. Phys. Chem. Solids* **113**, 17 (2018)
68. L.J. Cote, R. Cruz-Silva, J. Huang, *JACS* **131**, 11027 (2009)
69. E.E. Ghadim, N. Rashidi, S. Kimiagar, O. Akhavan, F. Manouchehri, E. Ghaderi, *Appl. Surf. Sci.* **301**, 183 (2014)
70. Y. Zhou, Q. Bao, L.A.L. Tang, Y. Zhong, K.P. Loh, *Chem. Mater.* **21**, 2950 (2009)
71. K. Ai, Y. Liu, L. Lu, X. Cheng, L. Huo, *J. Mater. Chem.* **21**, 3365 (2011)
72. C. Xu, X. Wang, J. Zhu, *J. Phys. Chem. C* **112**, 19841 (2008)
73. O. Akhavan, E. Ghaderi, *J. Phys. Chem. C* **113**, 20214 (2009)
74. M. Fernández-Merino, L. Guardia, J. Paredes, S. Villar-Rodil, P. Solís-Fernández, A. Martínez-Alonso, J. Tascón, *J. Phys. Chem. C* **114**, 6426 (2010)
75. C. Zhu, S. Guo, Y. Fang, S. Dong, *ACS Nano* **4**, 2429 (2010)
76. O. Akhavan, E. Ghaderi, S. Aghayee, Y. Fereydooni, A. Talebi, *J. Mater. Chem.* **22**, 13773 (2012)
77. J. Liu, S. Fu, B. Yuan, Y. Li, Z. Deng, *JACS* **132**, 7279 (2010)
78. A. Esfandiari, O. Akhavan, A. Irajizad, *J. Mater. Chem.* **21**, 10907 (2011)
79. O. Akhavan, M. Kalaei, Z. Alavi, S. Ghiasi, A. Esfandiari, *Carbon* **50**, 3015 (2012)
80. O. Akhavan, E. Ghaderi, E. Abouei, S. Hatamie, E. Ghasemi, *Carbon* **66**, 395 (2014)
81. S. Hatamie, O. Akhavan, S.K. Sadrnezhad, M.M. Ahadian, M.M. Shirolkar, H.Q. Wang, *Mater. Sci. Eng., C* **55**, 482 (2015)
82. O. Akhavan, E. Ghaderi, *Carbon* **50**, 1853 (2012)
83. O. Akhavan, *Carbon* **81**, 158 (2015)
84. P. Chamoli, M.K. Das, K.K. Kar, *J. Appl. Phys.* **122**, 185105 (2017)
85. P. Phillips, *Ann. Phys.* **321**, 1634 (2006)

86. P.R. Wallace, *Phys. Rev.* **71**, 622 (1947)
87. F. Bonaccorso, Z. Sun, T. Hasan, A. Ferrari, *Nat. Photonics* **4**, 611 (2010)
88. P. Avouris, *Nano Lett.* **10**, 4285 (2010)
89. Y.-W. Tan, Y. Zhang, K. Bolotin, Y. Zhao, S. Adam, E. Hwang, S.D. Sarma, H. Stormer, P. Kim, *Phys. Rev. Lett.* **99**, 246803 (2007)
90. K.I. Bolotin, K. Sikes, Z. Jiang, M. Klima, G. Fudenberg, J. Hone, P. Kim, H. Stormer, *Solid State Commun.* **146**, 351 (2008)
91. Y. Zhang, Y.-W. Tan, H.L. Stormer, P. Kim, *Nature* **438**, 201 (2005)
92. R.R. Nair, P. Blake, A.N. Grigorenko, K.S. Novoselov, T.J. Booth, T. Stauber, N.M. Peres, A.K. Geim, *Science* **320**, 1308 (2008)
93. F. Wang, Y. Zhang, C. Tian, C. Girit, A. Zettl, M. Crommie, Y.R. Shen, *Science* **320**, 206 (2008)
94. P.A. George, J. Strait, J. Dawlaty, S. Shivaraman, M. Chandrashekhara, F. Rana, M.G. Spencer, *Nano Lett.* **8**, 4248 (2008)
95. F. Rana, P.A. George, J.H. Strait, J. Dawlaty, S. Shivaraman, M. Chandrashekhara, M.G. Spencer, *Phys. Rev. B* **79**, 115447 (2009)
96. F. Xia, T. Mueller, Y.-M. Lin, A. Valdes-Garcia, P. Avouris, *Nat. Nanotechnol.* **4**, 839 (2009)
97. A.A. Balandin, *Nat. Mater.* **10**, 569 (2011)
98. D.G. Papageorgiou, I.A. Kinloch, R.J. Young, *Carbon* **95**, 460 (2015)
99. E. Pop, V. Varshney, A.K. Roy, *MRS Bull.* **37**, 1273 (2012)
100. C. Yu, L. Shi, Z. Yao, D. Li, A. Majumdar, *Nano Lett.* **5**, 1842 (2005)
101. S. Berber, Y.-K. Kwon, D. Tománek, *Phys. Rev. Lett.* **84**, 4613 (2000)
102. S. Ghosh, *Appl. Phys. Lett.* **92**, 151911 (2008)
103. I.-K. Hsu, M.T. Pettes, A. Bushmaker, M. Aykol, L. Shi, S.B. Cronin, *Nano Lett.* **9**, 590 (2009)
104. I. Frank, D. M. Tanenbaum, A. M. van der Zande, P. L. McEuen, *J. Vacuum Sci. & Technol. B: Microelectronics and Nanometer Structures Processing, Measurement, and Phenomena* **25**, 2558 (2007)
105. K.N. Kudin, G.E. Scuseria, B.I. Yakobson, *Phys. Rev. B* **64**, 235406 (2001)
106. C. Reddy, S. Rajendran, K. Liew, *Nanotechnol.* **17**, 864 (2006)
107. G. Van Lier, C. Van Alsenoy, V. Van Doren, P. Geerlings, *Chem. Phys. Lett.* **326**, 181 (2000)
108. M. Poot, H.S. van der Zant, *Appl. Phys. Lett.* **92**, 063111 (2008)
109. C. Gómez-Navarro, M. Burghard, K. Kern, *Nano Lett.* **8**, 2045 (2008)
110. D.A. Dikin, S. Stankovich, E.J. Zimney, R.D. Piner, G.H. Dommett, G. Evmenenko, S.T. Nguyen, R.S. Ruoff, *Nature* **448**, 457 (2007)
111. S. Park, D.A. Dikin, S.T. Nguyen, R.S. Ruoff, *J. Phys. Chem. C* **113**, 15801 (2009)
112. S. Park, K.-S. Lee, G. Bozoklu, W. Cai, S.T. Nguyen, R.S. Ruoff, *ACS Nano* **2**, 572 (2008)
113. R.J. Nicholl, H.J. Conley, N.V. Lavrik, I. Vlasiouk, Y.S. Puzryev, V.P. Sreenivas, S.T. Pantelides, K.I. Bolotin, *Nat. Commun.* **6**, 8789 (2015)
114. D.G. Papageorgiou, I.A. Kinloch, R.J. Young, *Prog. Mater. Sci.* **90**, 75 (2017)
115. A. Zandiatashbar, G.-H. Lee, S.J. An, S. Lee, N. Mathew, M. Terrones, T. Hayashi, C.R. Picu, J. Hone, N. Koratkar, *Nat. Commun.* **5**, 3186 (2014)
116. H. Qin, Y. Sun, J.Z. Liu, Y. Liu, *Carbon* **108**, 204 (2016)
117. P. Zhang, L. Ma, F. Fan, Z. Zeng, C. Peng, P.E. Loya, Z. Liu, Y. Gong, J. Zhang, X. Zhang, *Nat. Commun.* **5**, 3782 (2014)
118. P. Chamoli, M.K. Das, K.K. Kar, *Mater. Res. Exp.* **4**, 015012 (2017)
119. P. Chamoli, S.K. Singh, M. Akhtar, M.K. Das, K.K. Kar, *Physica E: Low-dimensional Syst. Nanostruct.* **103**, 25 (2018)
120. J. Dai, J. Yuan, P. Giannozzi, *Appl. Phys. Lett.* **95**, 232105 (2009)
121. L. Panchakarla, K. Subrahmanyam, S. Saha, A. Govindaraj, H. Krishnamurthy, U. Waghmare, C. Rao, *Adv. Mater.* **21**, 4726 (2009)
122. X. Wang, X. Li, L. Zhang, Y. Yoon, P.K. Weber, H. Wang, J. Guo, H. Dai, *Science* **324**, 768 (2009)
123. Y. Zou, F. Li, Z. Zhu, M. Zhao, X. Xu, X. Su, *Eur. Phys. J. B* **81**, 475 (2011)

124. T. Cui, R. Lv, Z.-H. Huang, H. Zhu, J. Zhang, Z. Li, Y. Jia, F. Kang, K. Wang, D. Wu, *Carbon* **49**, 5022 (2011)
125. R. Lv, T. Cui, M.S. Jun, Q. Zhang, A. Cao, D.S. Su, Z. Zhang, S.H. Yoon, J. Miyawaki, I. Mochida, *Adv. Funct. Mater.* **21**, 999 (2011)
126. L. Qu, Y. Liu, J.-B. Baek, L. Dai, *ACS Nano* **4**, 1321 (2010)
127. J. Carrero-Sanchez, A. Elías, R. Mancilla, G. Arrellin, H. Terrones, J. Laclette, M. Terrones, *Nano Lett.* **6**, 1609 (2006)
128. A.L. Elías, J.C. Carrero-Sánchez, H. Terrones, M. Endo, J.P. Laclette, M. Terrones, *Small* **3**, 1723 (2007)
129. Y. Wang, Y. Shao, D.W. Matson, J. Li, Y. Lin, *ACS Nano* **4**, 1790 (2010)
130. R. Lv, Q. Li, A.R. Botello-Méndez, T. Hayashi, B. Wang, A. Berkdemir, Q. Hao, A.L. Elías, R. Cruz-Silva, H.R. Gutiérrez, *Sci. Rep.* **2**, 586 (2012)
131. Z.-H. Sheng, H.-L. Gao, W.-J. Bao, F.-B. Wang, X.-H. Xia, *J. Mater. Chem.* **22**, 390 (2012)
132. J. Wang, R. Ma, Z. Zhou, G. Liu, Q. Liu, *Sci. Rep.* **5**, 9304 (2015)
133. Y. Zhu, S. Murali, W. Cai, X. Li, J.W. Suk, J.R. Potts, R.S. Ruoff, *Adv. Mater.* **22**, 3906 (2010)
134. B. H. Nguyen, V. H. Nguyen, *Adv. Natural Sci.: Nanosci. Nanotechnol.* **7**, 023002 (2016)
135. K.S. Novoselov, A.K. Geim, S. Morozov, D. Jiang, M. Katsnelson, I. Grigorieva, S. Dubonos, A.A. Firsov, *Nature* **438**, 197 (2005)
136. N. Mohanty, V. Berry, *Nano Lett.* **8**, 4469 (2008)
137. Y. Ohno, K. Maehashi, Y. Yamashiro, K. Matsumoto, *Nano Lett.* **9**, 3318 (2009)
138. S.K. Singh, P. Azad, M. Akhtar, K.K. Kar, *Mater. Res. Exp.* **4**, 086301 (2017)
139. L. Tang, Y. Wang, Y. Li, H. Feng, J. Lu, J. Li, *Adv. Funct. Mater.* **19**, 2782 (2009)
140. B.Z. Jang, A. Zhamu, *J. Mater. Sci.* **43**, 5092 (2008)
141. K. K. Kar, *Composite materials: processing, applications, characterizations* (Springer, 2016)
142. K. K. Kar, S. Rana, J. Pandey, *Handbook of polymer nanocomposites processing, performance and application* (Springer, 2015)
143. K. K. Kar, A. Hodzic, *Carbon nanotube based nanocomposites: recent developments* (Research Publishing Services, 2011)
144. M. Fang, K. Wang, H. Lu, Y. Yang, S. Nutt, *J. Mater. Chem.* **19**, 7098 (2009)
145. S. Ganguli, A.K. Roy, D.P. Anderson, *Carbon* **46**, 806 (2008)
146. K. Kalaitzidou, H. Fukushima, L.T. Drzal, *Compos. Sci. Technol.* **67**, 2045 (2007)
147. T. Ramanathan, A. Abdala, S. Stankovich, D. Dikin, M. Herrera-Alonso, R. Piner, D. Adamson, H. Schniepp, X. Chen, R. Ruoff, *Nat. Nanotechnol.* **3**, 327 (2008)